LAWRENCE
LIVERMORE
NATIONAL
LABORATORY

LLNL-JRNL-872416

Mechanically and chemically robust lanmodulin-functionalized silk sponges for rare earth element sequestration

L. Morton, J. Cotruvo, Y. Jiao, D. Park, D. Kaplan

February 13, 2025

ACS Biomaterials Science and Engineering

Disclaimer

Mechanically and chemically robust lanmodulin-functionalized silk sponges for rare earth element sequestration

Logan D. Morton[a], Ryan A. Scheel[a], Jugal Kishore Sahoo[a], Julian B. Gilbert[a], Joseph A. Cotruvo Jr. [b], Yongqin Jiao[c], Dan M. Park[c], David L. Kaplan[a*]

[a]Department of Biomedical Engineering, Tufts University, 4 Colby Street, Medford, Massachusetts 02155, United States

[b]Department of Chemistry, The Pennsylvania State University, University Park, PA 16802, United States

[c]Physical and Life Sciences Directorate, Lawrence Livermore National Laboratory, Livermore, California 94550, United States

[*]Corresponding Author: david.kaplan@tufts.edu

ABSTRACT

The extraction of rare-earth elements (REEs) from low-grade sources like electronic waste (E-waste) could supplement current unsustainable mining practices. REEs are crucial for various industries, but supply struggles to meet growing demand. Herein, we present an environmentally friendly method for REE extraction using silk protein sponges functionalized with lanmodulin (LanM), a protein that selectively binds REEs. These sponges are relatively facile to fabricate and scale, while offering highly selective REE binding. The REEs can then be recovered via simple acid leaching, allowing sponge reuse for multiple cycles as well as specific desorption of different REEs by changing the pH of the desorption buffer. This method avoids harmful solvents used in traditional extraction and enables recycling of REEs from industrial and E-waste.

KEYWORDS

REEs, silk, lanmodulin, E-waste, critical minerals, biomining, bioseparation

TABLE OF CONTENTS IMAGE

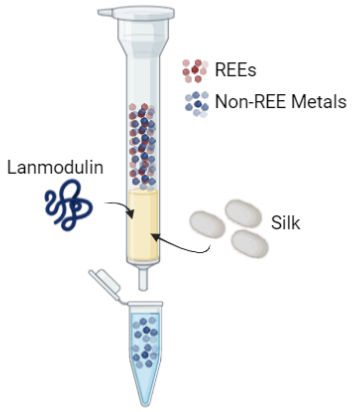

INTRODUCTION

The rare-earth elements (REEs), which include the lanthanides as well as scandium and yttrium, are indispensable to modern technology.[1] They are integral to a wide range of applications, from electronics to military defense systems, and are especially important in green energy technologies.[2,3] Despite their widespread use, the production of REEs is hampered by limited supply, widely varying natural abundance, and the geographic concentration of deposits.[1,2] Recent restrictions on REE exports by China due to rising domestic demand has heightened concerns about a global REE shortage.[4] The U.S. Department of Energy has even highlighted the urgent need for alternative REE sources.[5] Furthermore, current methods of REE production are environmentally harmful, relying heavily on mining and the use of toxic solvents, which generate substantial hazardous waste.[6,7] These practices undermine the benefits of REEs in green technologies. To address both supply and environmental challenges, alternative methods for REE extraction are being pursued, with a specific focus on solid–liquid extraction.[8] Solid-liquid extraction, which often involves immobilizing extractants onto supporting materials, enhances the contact area between the extractant and target elements. This approach improves extraction efficiency while mitigating issues like third-phase formation, a common problem in liquid-liquid extraction processes.

Recycling REEs from industrial and electronic waste (E-waste) is one promising strategy.[6,9,10] However, these waste streams often have high levels of impurities, necessitating highly efficient and selective separation techniques. This challenge has led to the exploration of a variety of different approaches for recovering REEs, including biological approaches such as bioleaching through the secretion of organic acids and biosorption through rare earth binding proteins, peptides and small-molecule ligands, and even with whole cell microorganisms.[11,12,21,22,13–20] Among the various extraction methods, solid-liquid separations based on biology-derived molecules have proven particularly attractive due to their ease of use, sustainability, and versatility.[18] In this context, we present a sustainable method for REE recovery using naturally derived silk sponges functionalized with lanmodulin, a highly selective lanthanide-binding protein derived from methylotrophic bacteria.[6,23–28]

Silk fibroin from the *Bombyx mori* silkworm, referred to from here on simply as silk, has been widely studied as a biomaterial system for applications in tissue engineering,[29–32] regenerative medicine,[33–35] drug delivery,[36–38] filtration,[19,39,40] and biosensing,[41,42] among others.[32,34] An extremely versatile material, silk can be processed into gels,[43,44] aerogels,[45,46] fibers,[31,35,47] particles,[37,48,49] sponges,[50,51] films,[52,53] and thermoplastics.[54,55] Furthermore, silk materials are a sustainably sourced raw material, enzymatically degradable and biocompatible. The silk sponges designed herein were formed from pre-functionalized LanM-Silk through thermally induced phase separation (TIPS) and were naturally porous enough to allow for moderate flow rates of REE solutions, while being easy to fabricate and scale to whatever dimensions are desired. Our data indicate that LanM-Silk is selective and effective for REE recovery, and silk represents an inexpensive and non-toxic substrate that can be used for protein immobilization in metal recovery applications.

METHODS

Materials

Chemical reagents were purchased from Thermo Fisher Scientific (Waltham, MA, USA) unless otherwise noted, at the highest purity available. Neodymium(III) chloride hydrate and dysprosium(III) chloride hydrate were dissolved in ultrapure water at 50 mM prior to dilution per the experimental conditions (usually to 0.2 mM). Lanthanum (III) chloride heptahydrate was purchased from Sigma Aldrich (St. Louis, MO, USA) and similarly stored at 50 mM prior to dilution.

All glassware used in filtration and REE analysis was rinsed 3 times with HCl (20 mM) and 3 times with DI water in between applications of REE solutions and oven-dried before reuse. All water samples for REE analysis were stored in HDPE 15 mL centrifuge tubes prior to analysis using inductively coupled plasma-optical emission spectroscopy (ICP-OES, Agilent). Neodymium and dysprosium ICP-OES standards (1000 ppm in 3% HNO_3) were purchased from Ricca Chemical and serially diluted with ultrapure water for calibration.

Silk fibroin preparation

Silk fibroin solution was prepared as described previously.[32] Briefly, unmodified *Bombyx mori* silkworm cocoons were cut into sections and the larva was removed. 5 g of the cut cocoons were boiled in a solution of sodium carbonate (Na_2CO_3) (4.24 g in 2 L of deionized (DI) water) for 30 minutes to remove the sericin protein from the fibroin. The resulting fibroin fibers were rinsed in DI water 3x for 20 minutes each and dried in a fume hood overnight. The next day, the silk fibroin was dissolved in 9.3 M lithium bromide (LiBr) and incubated at 60°C until dissolved. Once dissolved, the solution was dialyzed against DI water in a cellulose membrane (3.5 kDa MWCO) for 3 days changing the water 3-5 times per day. The solution was then collected, filtered through a 40 μm cell strainer to remove aggregates and centrifuged at 9,000 rpm for 20 min at 4°C. The silk solution was then transferred to new centrifuge tubes and centrifuged again to remove any other precipitate. To determine the concentration of the silk solution, 400 μL of solution was weighed and then allowed to dry into a film, at which time it was weighed again. The ratio of the wet and dry weight was used to determine the concentration. All silk solutions were stored at 4°C and used within 2 weeks.

Synthesis of silk fibroin-vinyl sulfone (SFVS)

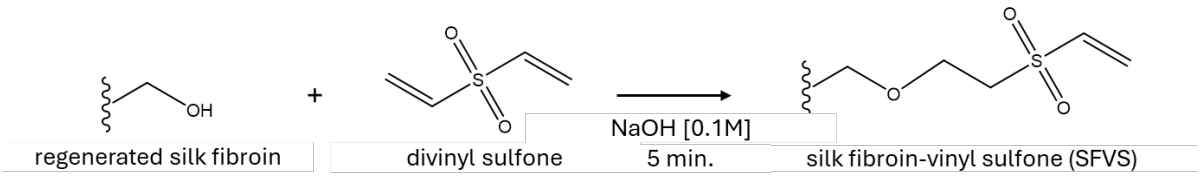

Scheme 1: Degummed silk fibroin is reacted with divinyl sulfone in a highly alkaline solution (pH~12.8) for 5 minutes.

Silk fibroin of a known concentration was first diluted to 2 wt% in water. Then, the quantity of serines (-OH groups) was determined via the following equation:

$$(1)\ M_{OH} = \frac{m_{SF}}{MW_{SF}} * \frac{M_{OH}}{1\ mole\ SF}$$

Where M_{OH} is the moles of hydroxyl groups (approximately 659), m_{SF} is the mass of silk fibroin in grams, and MW_{SF} is the molecular weight of the silk fibroin (assumed to be 417,000 g/mol). To calculate the requisite moles of divinyl sulfone, we used a stoichiometric ratio of $\frac{2.5M_{DVS}}{1M_{OH}}$ where M_{DVS} is the moles of divinyl sulfone. Thus, to determine the volume of divinyl sulfone necessary the following equation was used:

$$(2)\ V_{DVS} = \frac{M_{DVS}MW_{DVS}}{\rho_{DVS}}$$

Where V_{DVS} is the volume of the divinyl sulfone needed for the reaction, M_{DVS} is the moles of divinyl sulfone calculated from equation (1) and the stoichiometric ratio, MW_{DVS} is the molecular weight of divinyl sulfone (118.16 g/mol), and ρ_{DVS} is the density of divinyl sulfone (1.212 g/mL).

The silk was first added to a 0.1 M solution of NaOH while stirring at 1,500 rpm, while continually monitoring the pH (~12.8). Then, quickly, the divinyl sulfone was added to the stirring solution and allowed to react for 5 minutes.[56] Once complete, the reaction was quenched by neutralizing the pH to 7-7.4 by adding 1M HCl. The resulting vinyl sulfone-functionalized silk fibroin (SFVS) was dialyzed

against DI water in a cellulose membrane (3.5 kDa MWCO) for 3 days changing the water twice per day. The product was then frozen, lyophilized, and a small amount was dissolved in D_2O for proton nuclear magnetic resonance (^{1}H-NMR). To determine the degree of functionalization, the vinyl protons (around 6.9 ppm) were integrated and compared to the pre-functionalized silk fibroin.

Lanmodulin synthesis

The lanmodulin used in this study was the protein from *Methylobacterium extorquens*, containing a C-terminal GSGC addition for immobilization (called simply "LanM" subsequently), as described.[6] The plasmid containing the gene encoding this LanM was obtained from Twist Bioscience (pET-29b(+)-LanM-GSGC). The protein was overexpressed and purified in the CSL Behring Fermentation Facility, in the Huck Institutes of the Life Sciences at Penn State University. Pre-cultures of *E. coli* BL21(DE3) cells (NEB) transformed with pET-29b(+)-LanM-GSGC were grown first in 50 mL and then in 250 mL LB broth with 50 μg/mL kanamycin at 28 °C, from which 30 L of terrific broth (low P) was inoculated in a Sartorius Biostat Cplus fermentor with 30 L working volume. The media contained: 30 g/L tryptone, 40 g/L yeast extract, 30 g/L glycerol, 1 mM magnesium sulfate heptahydrate, 15.7 mM sodium phosphate monobasic, 9.9 mM potassium phosphate dibasic, and 50 μg/mL kanamycin. The pH was set to 6.8, with 20% dissolved oxygen (30 L/min air and 250-600 rpm agitation). The cells were grown at 37 °C to an OD_{600nm} of ~5, at which point isopropyl β-D-1-thiogalactopyranoside (IPTG) was added to 0.5 mM. After 3 h induction, cells were harvested at 16000 rpm using a Sharples AS-16 centrifuge. The yield was 1.0 kg cell paste, which was frozen at -80 °C. Purification was carried out as described previously.[6] Briefly, cells were lysed and loaded onto a Q-Sepharose Fast Flow column and eluted using a 0.01 to 1 M NaCl gradient. LanM-GSGC containing fractions were purified further using gel filtration chromatography (HiLoad 16/600 Superdex 75 pg column in 30 mM MOPS, 100 mM KCl, 5 mM $CaCl_2$, 5% glycerol, 5 mM TCEP, pH 7.0). LanM-GSGC-containing fractions were exchanged by FPLC into 20 mM acetate, 10 mM EDTA, 100 mM NaCl, 5% glycerol, pH 4.0, concentrated to ~3 mM, and frozen in liquid N_2 and stored at -80°C until use.

Quantifying lanmodulin concentration

To quantify the concentration of LanM in solution, an assay with Ellman's reagent was performed. Since the LanM protein is modified with a single cysteine we can directly correlate the thiol concentration to protein concentration in solution. First, a serial dilution was performed on a stock of cysteine at 2 mM, wherein the concentration was diluted by 50% several times yielding standards at 2, 1, 0.5, 0.25, 0.125, 0.0625, and 0.03125 mM. Each of these was added to a 96 well plate along with 5,5′-dithiobis-(2-nitrobenzoic acid) (Ellman's reagent). A noticeable color change was observed in each well. Simultaneously, LanM from the stock solution was added to the plate without dilution. All samples were measured for their absorbance of 412 nm light on a plate reader (Varioskan LUX Multimode Microplate Reader). The standards were then used to prepare a linear standard curve, which allowed us to calculate the LanM concentration from its absorbance.

Sponge fabrication

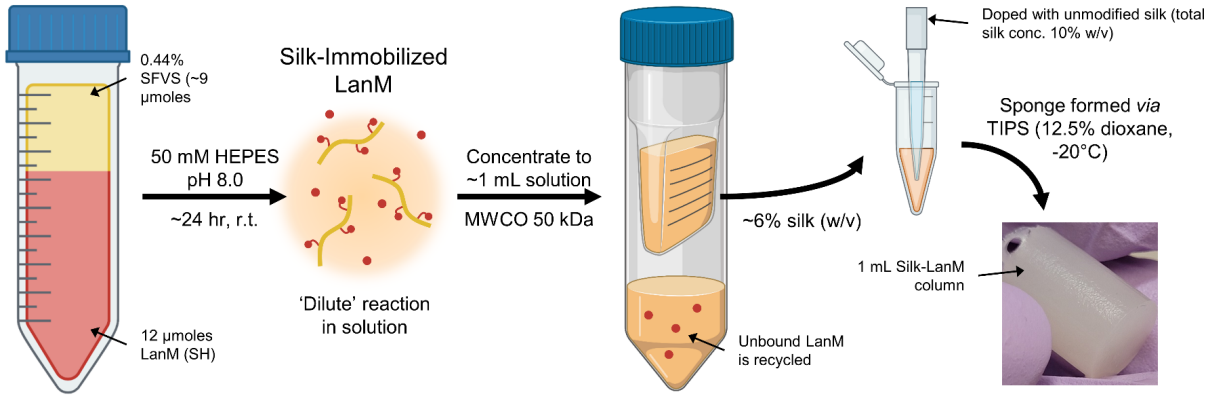

Scheme 2: SFVS is reacted with LanM in a dilute solution before concentrating, doping with unmodified silk, and freezing in a polydimethylsiloxane (PDMS) mold in the presence of 12.5% 1,4-dioxane overnight to allow for thermally induced phase separation (TIPS).

To prepare the LanM-tethered silk sponges, a dilute solution reaction between the SFVS (diluted to 0.44 wt%) and LanM was conducted for 24 hours at pH 7, 7.5, and 8 in 50 mM 2-[4-(2-hydroxyethyl)

piperazin-1-yl]ethanesulfonic acid (HEPES) buffer at room temperature. The solution was slowly rotated to ensure appropriate contact between the reactants. Each reaction was monitored by sodium dodecyl sulfate–polyacrylamide gel electrophoresis (SDS-PAGE) and Ellman's test (similar to what was described in the previous section to quantify unreacted LanM). The resulting solution was then concentrated using a 50 kDa MWCO centrifugal concentrator down to the appropriate volume for sponge preparation (~0.7 mL for a 1 mL sponge). Any unbound LanM was then recovered from the flow through. Then, a small volume of highly concentrated silk (>25 wt%) was added to bring the entire silk concentration to the appropriate concentration (usually 10 wt%). The 10 wt% silk was subsequently mixed with 50% dioxane at a ratio of 3:1 and frozen at -20°C overnight (unless otherwise stated) in a custom PDMS mold. The next morning the sponge was thawed and removed from the mold and was ready for use or further β sheeting if desired (see section below).

Morphological analysis of sponges

Sponges were prepared at a variety of different silk concentrations and freezing temperatures before being removed from the mold, lyophilized, and sliced into 100 μm sheets with a microtome blade. These sheets were then mounted on conductive adhesive tape and sputter-coated with a layer of Pt/Pd using a sputter coater (208HR, Cressington Scientific Instruments Inc.) prior to visualization with scanning electron microscopy (SEM, Zeiss UltraPlus SEM or Zeiss Supra 55 VP SEM, Carl Zeiss SMT Inc.). Images shown are representative of three sponges. The pore size distribution was then quantified using FIJI image analysis software to determine the average pore size for each condition.

Formation of β-sheets in silk sponges

A variety of treatments were investigated to induce β-sheet formation in the silk sponges to improve mechanical properties: 70% ethanol, 37˚C phosphate buffered saline (PBS), 37˚C water, and 0.5 M citrate buffer-pH 6. All treatments were then measured via Fourier Transform Infrared Spectroscopy (FTIR,

JASCO FTIR 6200 spectrometer), to quantify the amide I region, which corresponds to the presence of β-sheets.[57]

Rare earth element collection and separation

Sponges of different diameters (11 and 15 mm) and volumes (0.5, 1, 2, 5 mL) were prepared. These sponges were placed into custom-fitted columns to ensure secure housing and uniform flow distribution. The columns were attached directly to a peristaltic pump to facilitate consistent solution flow. A sponge size of 1 mL and 15 mm diameter with a flow rate of 2 mL/min was selected for most experiments, based on preliminary trials that optimized flow rate for minimal pressure drop, efficient REE recovery, and sufficient liquid/LanM interaction time. These conditions may provide insight into potential scale-up applications, where larger columns will be necessary. Care was taken to ensure that the REE solutions fully penetrated the sponge, and breakthrough curves were monitored to confirm efficient binding under these conditions. Unless otherwise stated, all data shown herein were collected under these optimized conditions.

For breakthrough experiments, a pure 0.2 mM solution of $LaCl_3$ in 1 mM HCl in water was flowed into the column for ~50 column volumes. As the solution was pumped through the sponge, flowthrough was collected in separate tubes as 1 mL fractions which were later analyzed for REE concentration by the arsenazo assay.[6,58]

To verify the point at which the REEs are no longer being captured, we monitored the REE concentration in 1 mL fractions over the course of 50 column volumes using an arsenazo assay. Arsenazo was dissolved in 6.25% trichloroacetic acid (TCA) to a final concentration of 0.1%. The solution was then filtered and stored protected from light until used. A 40 µL volume of each tube collected from the flowthrough was added to a 96 well plate along with 40 µL of 12.5% TCA and 120 µL of the arsenazo stock solution and allowed to incubate for 10 min at room temperature. Simultaneously, a standard curve of $LaCl_3$ was prepared ranging from 5 to 200 µM. The plate was then measured for absorbance at 652 nm using a plate

reader (Varioskan LUX Multimode Microplate Reader). Arsenazo changes color in the presence of metals and was a reliable means for determining the point at which the column's capacity was reached and La^{3+} began to flow through the column. This breakthrough point was then verified via Inductively Coupled Plasma Optical Emission spectroscopy (ICP-OES) (ICP-OES 5100, Agilent Technologies). Once the column was fully loaded, the La^{3+} was easily desorbed from the sponge through an acid desorption step with 12 mL of 25 mM HCl. This flowthrough was collected and analyzed by arsenazo and ICP-OES to verify the total loading capacity of the sponge.

Similarly, to determine the selectivity of the sponge-LanM system toward lanthanides, a competitive experiment between non-REE metals (Na^+, K^+) and La was performed, with the non-REEs being fed at 10x the concentration. The desorption step was conducted and analyzed by ICP-OES to quantify the amount of each metal that had been sequestered. Finally, separation of Nd and Dy was tested by flowing a mixed feed of equimolar $NdCl_3$ and $DyCl_3$ (0.2 mM) over the column. To specifically elute each REEs, a 2-step desorption was conducted: pH 2.1 for 20 column volumes (20 mL), followed by pH 1.7 for 20 column volumes, optimized desorption conditions developed previously.[6] The flowthrough from both of the desorption stages was collected and analyzed by ICP-OES to determine the concentrations of Nd and Dy at each point.

Statistics

The results are presented as a mean ± standard deviation where appropriate. Comparisons among groups were performed by one way analysis of variance (ANOVA) with post-hoc Tukey HSD test. Any conditions with $p<0.05$ were considered statistically significant.

RESULTS AND DISCUSSION

Silk fibroin-vinyl sulfone (SFVS) was prepared as previously described.[56] In short, silk cocoons were degummed and dissolved to extract regenerated silk fibroin, then the resulting silk fibroin was reacted with divinyl sulfone briefly in alkaline conditions. The resulting SFVS was reacted with LanM via thiol-

Michael addition overnight. This silk functionalization was found to be highly pH dependent, as shown in **Figure 1**. The kinetics of the reaction varied significantly across pH conditions, with faster rates observed at higher pH levels. At pH 7, thiol loss occurred gradually, as indicated by the relatively shallow slope (~0.4 mM/hour) in the initial phase, stabilizing at a higher free thiol concentration (~0.2 mM) after 8 hours (**Figure 1B**). This is confirmed in the third gel (**Figure 1A**) wherein bands are visible throughout the entire reaction time. In contrast, pH 7.5 exhibited a steeper initial decline (~0.8 mM/hour), indicating accelerated thiol reactivity (**Figure 1B**), which was mirrored by a decrease in visible bands toward the later hours of the reaction (**Figure 1A**). Finally, pH 8 demonstrated the fastest reaction rate, with a steep initial slope (~1 mM/hour) and stabilization at the lowest thiol concentration (~0.1 mM) (**Figure 1B**). This too was confirmed by SDS-Page in the first gel (**Figure 1A**) which has no visible bands toward the end of the reaction time. These trends suggest that higher pH enhances thiol reactivity, likely due to the increased nucleophilicity of thiolate anions, which contributes to superior functionalization of the silk.

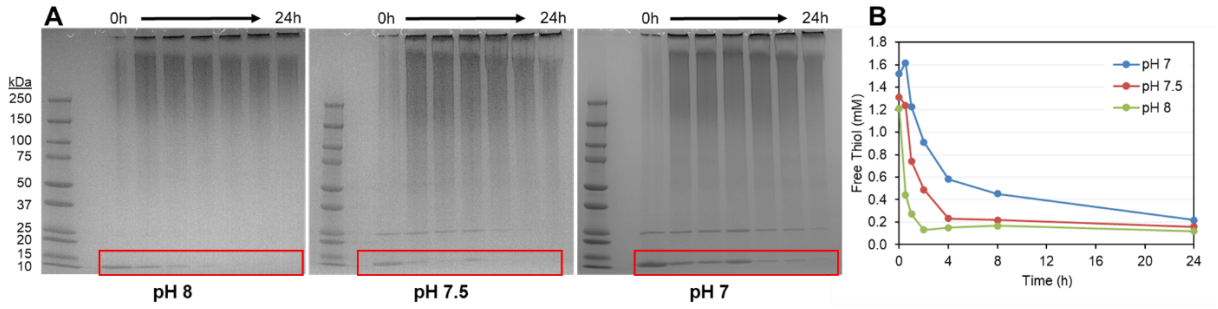

Figure 1. A. SDS-PAGE of each reaction (pH 7, 7.5, and 8) between LanM and SFVS. Time points were taken at 0, 0.1, 1, 2, 4, 8, and 24 h. Note that LanM is ~12 kDa, so it is represented by the first visible bands on the bottom of the images. With increasing pH, the quantity of LanM remaining unreacted decreases at every timepoint measured. **B.** Ellman's assay at various points (0, 0.1, 1, 2, 4, 8, and 24 h) during each experiment. This verifies the finding with SDS-PAGE that the reaction is faster at higher pH.

The SFVS-LanM product was then concentrated to ~70% of the desired sponge volume using centrifugal concentrators with 50-kDa molecular weight cutoff, which allowed any unreacted LanM to pass through the filter. The flowthrough was measured by Ellman's reagent to quantify the amount of unreacted LanM, which was usually less than 5% of the initial LanM added. The resulting concentrated SFVS-LanM was

then enriched with >25 wt% silk to bring it to the proper final concentration (2.5-20 wt%) before mixing with 1,4-dioxane and frozen overnight to induce TIPS. Significant morphological and mechanical differences were observed as the silk concentration was altered. Namely, the softest sponges (2.5 and 5 wt%) appeared to have their pores collapse under their own weight due to their weak mechanics, while the stiffest sponges (15 wt% and 20 wt%) had the largest pores that substantially decreased their surface area as well as the residence time of solutions passing through them (**Figure 2**). The 10 wt% sponges were found to have the microstructure that best balanced mechanics and flowrate through the sponge.

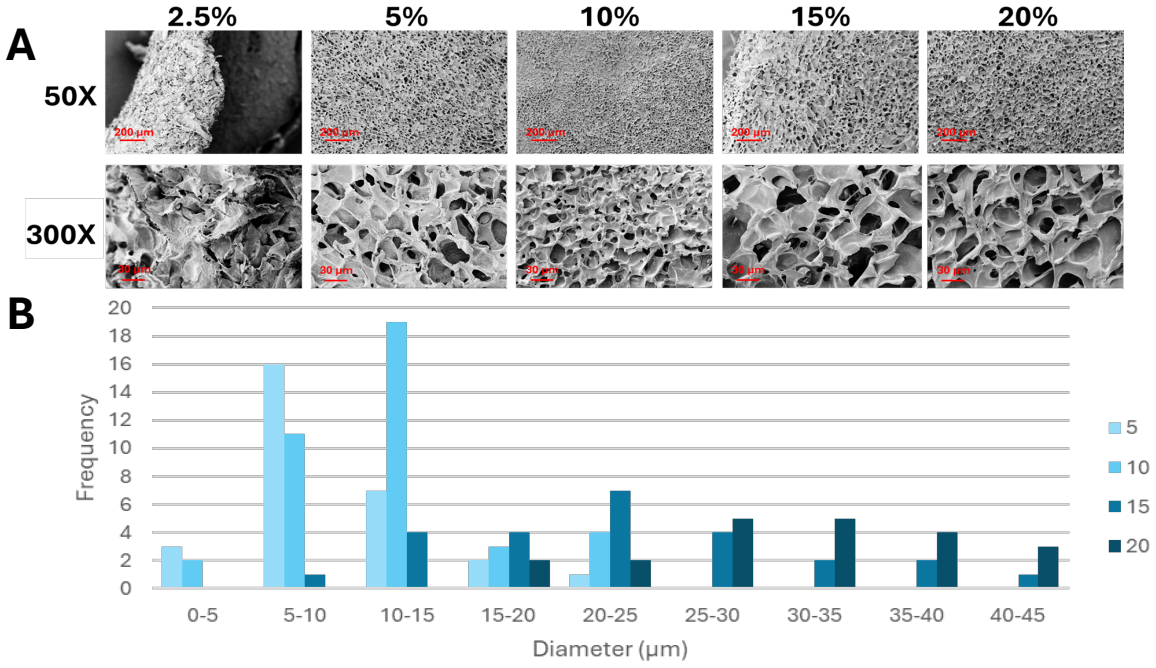

Figure 2. Microstructure of sponges formed at a variety of silk concentrations (2.5, 5, 10, 15, and 20 wt%) visualized via scanning electron microscopy at two different magnifications (50X and 300X). **A.** Clear morphological differences were present in most conditions, with 2.5-5 wt% sponges seeming to collapse internally due to their poor mechanics and 15 and 20 wt% sponges having pores that led to decreased LanM-REE interactions due to their larger size. 10 wt% sponges were determined to be the best suited for this application and were thus used in all subsequent experiments. Scale bars are 200 μm in the top images and 30 μm in the bottom images. **B.** Pore size quantification of each sponge ranging from 5 to 20 wt% silk. Note that the 2.5 wt% sponges were not measured due to the pores collapsing before imaging.

Different freezing temperatures also resulted in different microstructures (**Figure 3**). Freezing at -80˚C resulted in, on-average, large pores that resulted in limited residence time. Alternatively, freezing in liquid

nitrogen (-196˚C) resulted in very small pores that entirely prevented flow through the sponge. Additionally, the -196˚C sponge was far more brittle than the sponges frozen at the higher temperatures, resulting in cracking and damage due to handling. A freezing temperature of -20˚C resulted in interconnected pores that provided the proper tortuosity to allow for reasonable flowrates (>2 mL/min) that still promoted sufficient REE-LanM interactions.

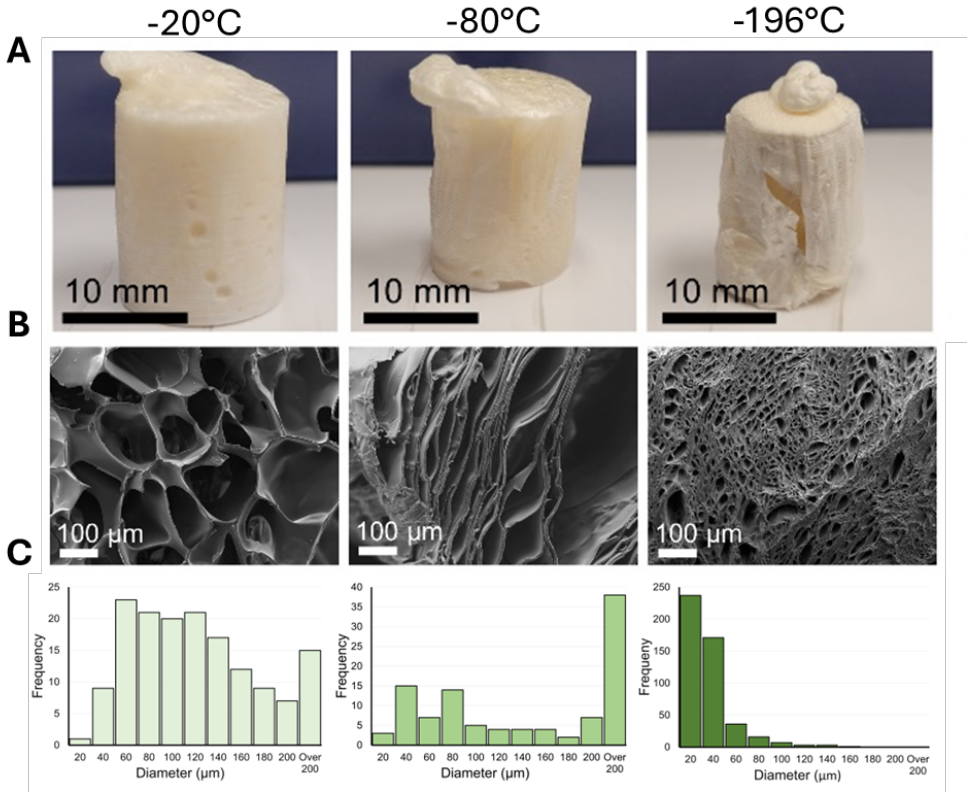

Figure 3. A. Images of sponges (10 wt% silk) formed via 3 different freezing rates (-20˚C, -80˚C, and -196˚C), showing some damage on the most brittle sponge (the one frozen in -196˚C) **B.** Sponge microstructure visualized via scanning electron microscopy, indicating substantial differences in pore size. **C.** Pore size quantification for each sponge.

After fabricating the sponges, subsequent β-sheet formation was conducted through multiple, well-documented treatments: ethanol, 37˚C water, 37˚C PBS, and citrate. β-sheeting in silk sponges provides mechanical strength and structural stability, essential for maintaining shape and integrity under stress. It also enhances resistance to enzymatic degradation, ensuring long-term stability in relevant environments. While all treatments significantly increased the β-sheet content, as measured by FTIR, 37˚C water

resulted in the highest percentage of β-sheeting (**Figure 4B**) and was used for all subsequently fabricated sponges. Notably, this degree of β-sheeting aligns with β-sheet content measured in previous silk sponges and in other silk materials (films, electrospun fibers, etc.) more broadly.

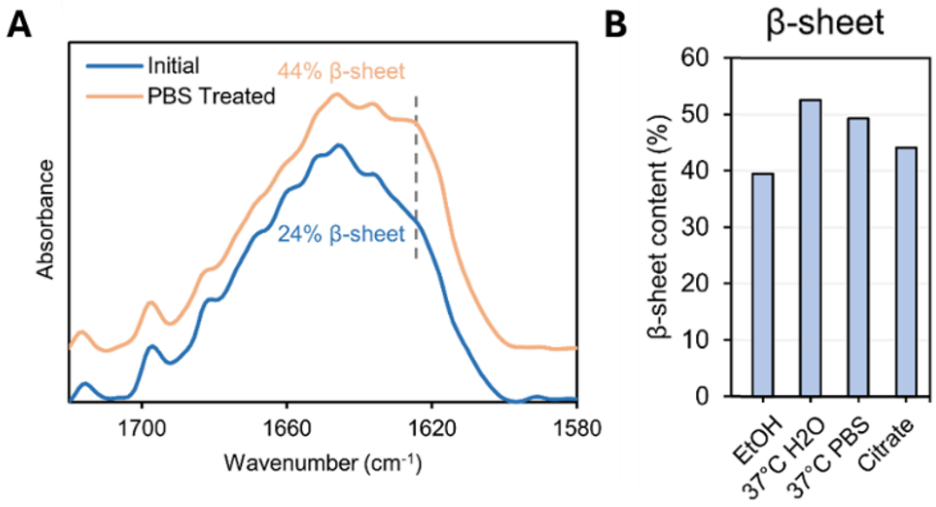

Figure 4. A. Representative FTIR illustrating the difference in the amide I region before and after treatment with PBS. **B.** β-sheet content, as measured by FTIR, for 4 different treatments (70% EtOH, 37˚C water, 37˚C PBS, and 0.5M Citrate buffer-pH 6), illustrating that 37˚C water results in the largest increase.

Initially, the sponges were fabricated in an 11-mm-diameter PDMS mold and placed into a column connected to a peristaltic pump, which slowly pumped a solution of 0.2 mM $LaCl_3$ through the sponge. The flowthrough was collected and the La concentration was measured, confirming that no substantial breakthrough of La was observed until ~20 column volumes. This translates to approximately 4 μmol La captured before breakthrough (**Figure 5A**). We performed acid desorption to quantify the total La adsorption capacity of the sponge column, which also includes La captured post-breakthrough, up to 50 mL. Based on **Figure 5B**, the sponge exhibits an adsorption capacity of around 10 μmol/mL, which corresponds to roughly one mole of La bound per mole of LanM attached to the sponge. Because prior studies have reported higher ratios (up to 2:1 REE:LanM), this finding suggests that some LanM may be nonfunctional—possibly because certain LanM molecules are shielded from interacting with the La in the flowthrough. Notably, these findings were replicated for an additional 2 cycles, addressing the reusability of the sponges.

To determine the specificity of the LanM sponges for REE binding, a mixed feed of $LaCl_3$, NaCl, and KCl was prepared, with both NaCl and KCl at concentrations 10-fold higher than the $LaCl_3$. After a full 50 mL loading onto the column, negligible Na^+ and K^+ were observed, indicating that >99.994% of the bound metal was La (**Figure 5C, Table S1**). Additionally, we repeated this experiment with silk sponges that lacked the LanM functionalization and found minimal to no adsorption of any of the 3 metals (**Table S2**).

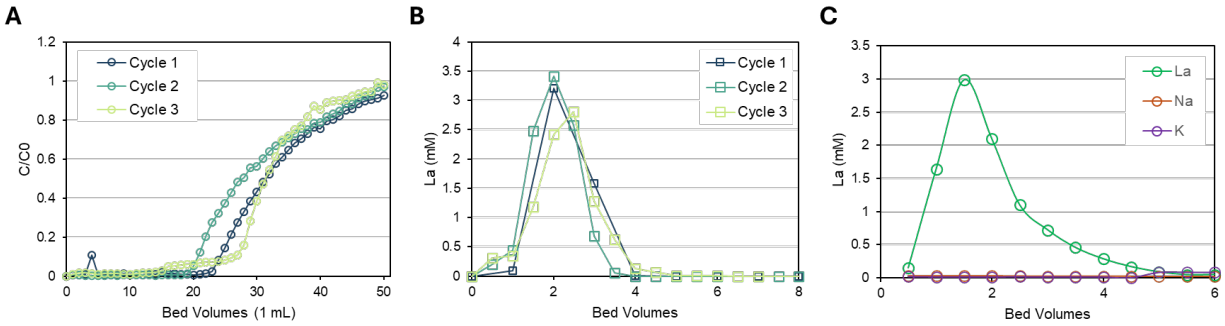

Figure 5. A. Breakthrough curves of $LaCl_3$ (pH 3) pumped through the sponges, indicating no substantial La breaking through the sponge until ~20 column volumes for 3 adsorption/desorption cycles. **B.** Desorbed La from the column (using 25 mM HCl—pH ~1.6) over 3 cycles, showing approximately 10 µmol La were bound in total. **C.** A mixed feed experiment containing 3 metals demonstrating the high selectivity of these LanM silk sponges toward REE sequestration.

We hypothesized that early La breakthrough occurred because of the La traveling through the same few tortuous pathways through the sponge, which could be ameliorated by increasing the cross-sectional area of the sponge by increasing its diameter, without altering its volume. Toward this end, we fabricated new sponges in a PDMS mold with a diameter of 15 mm. These larger sponges were then tested via a similar $LaCl_3$ flowthrough experiment, and it was found that, indeed, the breakthrough was improved to ~24-30 column volumes (**Figure 6A**).

Lastly, we endeavored to discover the potential to not only capture, but also separate REEs using a single sponge adsorption system. A 50/50 mixture of $NdCl_3$ and $DyCl_3$ were fed to the column and allowed to adsorb for 50 column volumes, before being desorbed in a staged desorption system. Initially, 20 mL of pH 2.1 desorption buffer was pumped through the column to desorb the Dy, followed by an additional 20 mL of desorption buffer at pH 1.7. Two distinct peaks, one at the beginning of each pH range, were

visible when quantifying the metal ion concentration of the eluted fractions using arsenazo. As expected based on characterization of LanM in solution[23] and immobilized on agarose beads[6], the Dy was desorbed first, and was verified to be >95% pure by ICP-OES (**Figure 6B, Table S3**). Neodymium was collected in the second stage of the desorption process at 95% purity as well (**Figure 6B**). This confirmed that these sponges could be used not only to extract REEs, but also to separate certain REEs based on their differential affinity to LanM.

These results are consistent with expectations based on previous work in the field, demonstrating comparable performance to established methods for REE separation. Prior studies, such as those by Cotruvo et al. and Dong et al.,[23,28] showed that LanM is highly selective for REEs like Dy and Nd, with purities exceeding 95% achieved in both solution-based systems and agarose bead immobilization setups. These results using silk sponges align with this benchmark, as Dy and Nd were desorbed sequentially with >95% purity, highlighting the reliability of LanM's differential affinity for REEs.

The sponges developed in this work exhibit an REE binding capacity of ~10 μmol/mL, surpassing agarose bead-based systems (~5.77 μmol/mL for Nd^{3+}) while demonstrating higher operational flow rates (2 mL/min), making them well-suited for high-throughput applications.[6] However, each competing REE sequestration approach offers distinct advantages. Agarose bead immobilization, as demonstrated by Dong et al., provides a well-characterized and widely used platform that enables precise control over column separations and facilitates easy integration into existing purification infrastructure. The beads' stability and high selectivity make them particularly useful for batch or continuous chromatography applications, though their diffusion-limited binding kinetics and lower flowrate capacity may restrict throughput. Elastin-like polypeptide (ELP) conjugates, as reported by Hussain et al., present a highly innovative approach by leveraging thermoresponsive phase separation to enable simple REE recovery via temperature-induced precipitation.[9] This phase transition mechanism eliminates the need for harsh chemical desorption steps, allowing for easy recyclability of the material. While this strategy offers significant advantages in terms of ease of recovery and reusability, its adsorption capacity per unit volume

appears lower than that of the sponge-based system, and the aggregation behavior of ELPs could pose challenges in large-scale deployment. Cell surface immobilization, explored by Park et al., represents a promising solution for biomining applications, where engineered microbial systems express LBTs on their surfaces to continuously extract REEs from dilute sources.[59] This approach excels in in situ applications, as it does not require pre-synthesized materials and benefits from the self-replicating nature of bacterial cultures. However, REE recovery from requires complicating downstream purification, potentially limiting the ease of REE extraction in industrial settings.

Beyond biomolecular methods, traditional industrial REE extraction technologies remain the dominant approach. Liquid-liquid extraction (LLE), as described by Pramanik et al.[1], is a highly efficient and scalable method widely employed in commercial REE refining. By leveraging organic phase separation and selective ligands, LLE effectively extracts REEs from complex matrices. However, its dependence on toxic organic solvents and the generation of large volumes of hazardous waste raise environmental and operational concerns. In contrast, ion exchange resins, as discussed by Jordens et al.[3], offer a reusable and highly selective alternative, making them a key component of hydrometallurgical REE recovery. Despite their efficacy, ion exchange resins are prone to fouling, require costly regeneration, and may have limited throughput when processing complex feedstocks.

In comparison, the silk fibroin sponge system developed in this work presents a promising bio-based alternative that combines high adsorption capacity, scalability, and sustainability. Unlike agarose beads, the sponge system supports higher flow rates and improved adsorption kinetics. While ELP conjugates offer an efficient phase-separation recovery mechanism, the silk-based system achieves greater adsorption per unit volume. Similarly, while cell surface immobilization is advantageous for biomining applications, the sponge system provides a more straightforward recovery process. Compared to LLE and ion exchange resins, which remain the gold standard for industrial-scale REE separations, the sponge system eliminates the need for toxic solvents or synthetic polymer resins, reducing environmental impact while maintaining a competitive binding capacity.

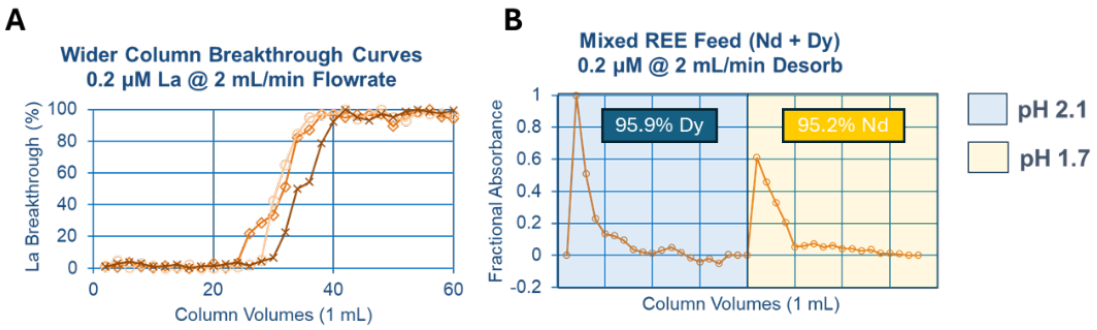

Figure 6. A. Breakthrough curves from 15 mm diameter, 1 mL sponges, indicating a marked improvement over the 11 mm diameter sponges shown previously. These are data from 3 independent runs, with the darker colors being the later runs, indicating no drop off in performance. **B.** Analysis of a mixed Nd/Dy feed loaded onto the LanM silk sponges and separated by a simple 2 stage desorption (pH 2.1, then 1.7) showing two distinct peaks, each of which is >95% pure in either Dy or Nd, respectively.

CONCLUSIONS

The growing demand for REEs in modern technology and green energy solutions, coupled with supply limitations and environmentally harmful extraction methods, necessitates the development of sustainable and efficient recovery techniques. Herein, we designed a naturally derived silk protein sponge system functionalized with LanM, a highly selective lanthanide-binding protein, as a promising solution to these challenges. This method leverages the inherent versatility and processability of silk fibroin from the *Bombyx mori* silkworm, which can be easily fabricated and scaled to meet demand based on the large silk production infrastructure already in place worldwide to generate silk for textiles via sericulture. The TIPS fabrication process enabled the creation of porous silk sponges that facilitate flow rates >2 mL/min of REE solutions, thereby enhancing the practicality and efficiency of REE recovery. Other sponge poration processes may be amenable to REE recovery,[32,34] but we believe that TIPS-based sponges result in pores that are an ideal balance of flow rate and surface area. For metal extraction applications, the chosen parameter matrix (e.g., 15 mm diameter, 1 mL sponge volume) provided the best compromise between scalability, efficiency of target ion binding, and durability during continuous flow. These design considerations were informed by both experimental data and the requirements for potential scale-up, emphasizing the importance of achieving a balance between structural properties and functional

performance. For scaled up versions of this system, we believe it to be imperative to keep the ratio of diameter:volume approximately 15:1.

Our findings underscore the potential of LanM-Silk sponges as a sustainable alternative to traditional REE extraction methods, combining ease of use, environmental friendliness, and high selectivity. This approach not only addresses the urgent need for alternative REE sources but also aligns with global efforts to reduce the environmental impact of REE production. Future research and development should focus on optimizing the fabrication process, improving the selectivity and capacity of the sponges, and exploring the scalability of this technology for industrial applications. By advancing such sustainable technologies, we can mitigate the environmental footprint of REE extraction and secure a reliable supply of these critical elements for the advancement of modern and green technologies.

ACKNOWLEDGEMENTS

We would like to gratefully acknowledge Tim McClure with the Massachusetts Institute of Technology (MIT) Materials Research Laboratory for his training and assistance with the ICP-OES analysis. The authors would like to acknowledge the Huck Institutes' CSL-Behring Fermentation Core Facility (RRID:SCR_024459) at the Pennsylvania State University for use of the Sartorius Biostat Cplus fermentor and Sharples AS-16 centrifuge and staff Yawen Song Anderson for expression of the LanM protein used in these studies. We also thank Joseph A. Mattocks (Pennsylvania State University) for purification of LanM. The TOC image and Scheme 2 were created with assets from BioRender.com.

FUNDING SOURCES

This work was funded by the DARPA Environmental Microbes as a Bioengineering Resource (EMBER) program (contract DE-AC52-07NA27344). The views, opinions, and/or findings expressed are those of the authors and should not be interpreted as representing the official views or policies of the Department of Defense or the U.S. Government. Distribution Statement A - Approved for Public Release, Distribution

Unlimited. Contributions from D.M.P and Y.J. were carried out under the auspices of the DOE by Lawrence Livermore National Laboratory under contract DEAC52-07NA27344 (LLNL-JRNL-872416).

REFERENCES

(1) Pramanik, B. K.; Nghiem, L. D.; Hai, F. I. Extraction of Strategically Important Elements from Brines: Constraints and Opportunities. *Water Res.* **2020**, *168*, 115149. https://doi.org/https://doi.org/10.1016/j.watres.2019.115149.

(2) Drobniak, A.; Mastalerz, M. Rare Earth Elements: A Brief Overview. *Indiana J. Earth Sci.* **2022**, *4*.

(3) Jordens, A.; Cheng, Y. P.; Waters, K. E. A Review of the Beneficiation of Rare Earth Element Bearing Minerals. *Miner. Eng.* **2013**, *41*, 97–114. https://doi.org/https://doi.org/10.1016/j.mineng.2012.10.017.

(4) Kose Mutlu, B.; Cantoni, B.; Turolla, A.; Antonelli, M.; Hsu-Kim, H.; Wiesner, M. R. Application of Nanofiltration for Rare Earth Elements Recovery from Coal Fly Ash Leachate: Performance and Cost Evaluation. *Chem. Eng. J.* **2018**, *349*, 309–317. https://doi.org/https://doi.org/10.1016/j.cej.2018.05.080.

(5) Bauer, D.; Khazdozian, H.; Mehta, J.; Nguyen, R. T.; Severson, M. H.; Vaagensmith, B. C.; Toba, L.; Zhang, B.; Hossain, T.; Sibal, A. P. *2023 Critical Materials Strategy*; Idaho National Laboratory (INL), Idaho Falls, ID (United States), 2023.

(6) Dong, Z.; Mattocks, J. A.; Deblonde, G. J.-P.; Hu, D.; Jiao, Y.; Cotruvo, J. A. J.; Park, D. M. Bridging Hydrometallurgy and Biochemistry: A Protein-Based Process for Recovery and Separation of Rare Earth Elements. *ACS Cent. Sci.* **2021**, *7* (11), 1798–1808. https://doi.org/10.1021/acscentsci.1c00724.

(7) Wang, L.; Huang, X.; Yu, Y.; Xiao, Y.; Long, Z.; Cui, D. Eliminating Ammonia Emissions during Rare Earth Separation through Control of Equilibrium Acidity in a HEH(EHP)-Cl System. *Green Chem.* **2013**, *15* (7), 1889–1894. https://doi.org/10.1039/C3GC40470F.

(8) Hidayah, N. N.; Abidin, S. Z. The Evolution of Mineral Processing in Extraction of Rare Earth Elements Using Solid-Liquid Extraction over Liquid-Liquid Extraction: A Review. *Miner. Eng.* **2017**, *112*, 103–113. https://doi.org/https://doi.org/10.1016/j.mineng.2017.07.014.

(9) Hussain, Z.; Kim, S.; Cho, J.; Sim, G.; Park, Y.; Kwon, I. Repeated Recovery of Rare Earth Elements Using a Highly Selective and Thermo-Responsive Genetically Encoded Polypeptide. *Adv. Funct. Mater.* **2022**, *32* (13), 2109158. https://doi.org/https://doi.org/10.1002/adfm.202109158.

(10) Liang, J.; Zhang, X.; Li, H.; Wen, C.; Tian, L.; Chen, X.; Li, Z. Constructing Two-Dimensional (2D) Heterostructure Channels with Engineered Biomembrane and Graphene for Precise Scandium Sieving. *Adv. Mater.* **2024**, *36* (30), 2404629. https://doi.org/https://doi.org/10.1002/adma.202404629.

(11) Kubota, F.; Shimobori, Y.; Baba, Y.; Koyanagi, Y.; Shimojo, K.; Kamiya, N.; Goto, M. Application of Ionic Liquids to Extraction Separation of Rare Earth Metals with an Effective Diglycol Amic Acid Extractant. *J. Chem. Eng. Japan* **2011**, *44* (5), 307–312.

(12) Kubota, F.; Baba, Y.; Goto, M. Application of Ionic Liquids for the Separation of Rare Earth Metals. *Solvent Extr. Res. Dev. Japan* **2012**, *19*, 17–28.

(13) Yan, C.; Jia, J.; Liao, C.; Wu, S.; Xu, G. Rare Earth Separation in China. *Tsinghua Sci. Technol.* **2006**, *11* (2), 241–247.

(14) Xie, F.; Zhang, T. A.; Dreisinger, D.; Doyle, F. A Critical Review on Solvent Extraction of Rare Earths from Aqueous Solutions. *Miner. Eng.* **2014**, *56*, 10–28.

(15) Liu, Y.; Chen, J.; Li, D. Application and Perspective of Ionic Liquids on Rare Earths Green Separation. *Sep. Sci. Technol.* **2012**, *47* (2), 223–232.

(16) Takahashi, Y.; Châtellier, X.; Hattori, K. H.; Kato, K.; Fortin, D. Adsorption of Rare Earth Elements onto Bacterial Cell Walls and Its Implication for REE Sorption onto Natural Microbial Mats. *Chem. Geol.* **2005**, *219* (1–4), 53–67.

(17) Chunsheng, L.; Sheng, W. U.; Cheng, F.; Songling, W.; Yan, L. I. U.; Zhang, B.; Chunhua, Y. A. N. Clean Separation Technologies of Rare Earth Resources in China. *J. Rare Earths* **2013**, *31* (4), 331–336.

(18) Chen, L.; Wu, Y.; Dong, H.; Meng, M.; Li, C.; Yan, Y.; Chen, J. An Overview on Membrane Strategies for Rare Earths Extraction and Separation. *Sep. Purif. Technol.* **2018**, *197*, 70–85. https://doi.org/https://doi.org/10.1016/j.seppur.2017.12.053.

(19) Scheel, R. A.; Sahoo, J. K.; Morton, L. D.; Xia, Z.; Blum, J. R.; Martin-Moldes, Z.; Kaplan, D. L. Reusable Silk-Based Mesoporous Membranes for Recovery of Rare-Earth Elements. *ACS ES&T Eng.* **2024**. https://doi.org/10.1021/acsestengg.4c00184.

(20) Verma, G.; Hostert, J.; Summerville, A. A.; Robang, A. S.; Garcia Carcamo, R.; Paravastu, A. K.; Getman, R. B.; Duval, C. E.; Renner, J. Investigation of Rare Earth Element Binding to a Surface-Bound Affinity Peptide Derived from EF-Hand Loop I of Lanmodulin. *ACS Appl. Mater. Interfaces* **2024**, *16* (13), 16912–16926. https://doi.org/10.1021/acsami.3c17565.

(21) Medin, S.; Dressel, A.; Specht, D. A.; Sheppard, T. J.; Holycross, M. E.; Reid, M. C.; Gazel, E.; Wu, M.; Barstow, B. Multiple Rounds of In Vivo Random Mutagenesis and Selection in Vibrio Natriegens Result in Substantial Increases in REE Binding Capacity. *ACS Synth. Biol.* **2023**, *12* (12), 3680–3694. https://doi.org/10.1021/acssynbio.3c00484.

(22) Gut, M.; Wilhelm, T.; Beniston, O.; Ogundipe, S.; Kuo, C.-C.; Nguyen, K.; Furst, A. Lanmodulin-

Decorated Microbes for Efficient Lanthanide Recovery. *Adv. Mater.* **2025**, *n/a* (n/a), 2412607. https://doi.org/https://doi.org/10.1002/adma.202412607.

(23) Cotruvo, J. A. J.; Featherston, E. R.; Mattocks, J. A.; Ho, J. V; Laremore, T. N. Lanmodulin: A Highly Selective Lanthanide-Binding Protein from a Lanthanide-Utilizing Bacterium. *J. Am. Chem. Soc.* **2018**, *140* (44), 15056–15061. https://doi.org/10.1021/jacs.8b09842.

(24) Cook, E. C.; Featherston, E. R.; Showalter, S. A.; Cotruvo, J. A. J. Structural Basis for Rare Earth Element Recognition by Methylobacterium Extorquens Lanmodulin. *Biochemistry* **2019**, *58* (2), 120–125. https://doi.org/10.1021/acs.biochem.8b01019.

(25) Deblonde, G. J.-P.; Mattocks, J. A.; Park, D. M.; Reed, D. W.; Cotruvo, J. A. J.; Jiao, Y. Selective and Efficient Biomacromolecular Extraction of Rare-Earth Elements Using Lanmodulin. *Inorg. Chem.* **2020**, *59* (17), 11855–11867. https://doi.org/10.1021/acs.inorgchem.0c01303.

(26) Featherston, E. R.; Issertell, E. J.; Cotruvo, J. A. J. Probing Lanmodulin's Lanthanide Recognition via Sensitized Luminescence Yields a Platform for Quantification of Terbium in Acid Mine Drainage. *J. Am. Chem. Soc.* **2021**, *143* (35), 14287–14299. https://doi.org/10.1021/jacs.1c06360.

(27) Deblonde, G. J.-P.; Mattocks, J. A.; Wang, H.; Gale, E. M.; Kersting, A. B.; Zavarin, M.; Cotruvo, J. A. J. Characterization of Americium and Curium Complexes with the Protein Lanmodulin: A Potential Macromolecular Mechanism for Actinide Mobility in the Environment. *J. Am. Chem. Soc.* **2021**, *143* (38), 15769–15783. https://doi.org/10.1021/jacs.1c07103.

(28) Dong, Z.; Mattocks, J. A.; Seidel, J. A.; Cotruvo, J. A.; Park, D. M. Protein-Based Approach for High-Purity Sc, Y, and Grouped Lanthanide Separation. *Sep. Purif. Technol.* **2024**, *333*, 125919. https://doi.org/https://doi.org/10.1016/j.seppur.2023.125919.

(29) Gupta, A. K.; Coburn, J. M.; Davis-Knowlton, J.; Kimmerling, E.; Kaplan, D. L.; Oxburgh, L. Scaffolding Kidney Organoids on Silk. *J. Tissue Eng. Regen. Med.* **2019**, *13* (5), 812–822.

https://doi.org/10.1002/term.2830.

(30) Sahoo, J. K.; Hasturk, O.; Choi, J.; Montero, M. M.; Descoteaux, M. L.; Laubach, I. A.; Kaplan, D. L. Sugar Functionalization of Silks with Pathway-Controlled Substitution and Properties. *Adv. Biol.* **2021**, *5* (7), 2100388. https://doi.org/https://doi.org/10.1002/adbi.202100388.

(31) Li, C.; Vepari, C.; Jin, H. J.; Kim, H. J.; Kaplan, D. L. Electrospun Silk-BMP-2 Scaffolds for Bone Tissue Engineering. *Biomaterials* **2006**, *27* (16), 3115–3124. https://doi.org/10.1016/j.biomaterials.2006.01.022.

(32) Rockwood, D. N.; Preda, R. C.; Yücel, T.; Wang, X.; Lovett, M. L.; Kaplan, D. L. Materials Fabrication from Bombyx Mori Silk Fibroin. *Nat. Protoc.* **2011**, *6* (10), 1612–1631. https://doi.org/10.1038/nprot.2011.379.

(33) Sahoo, J. K.; Choi, J.; Hasturk, O.; Laubach, I.; Descoteaux, M. L.; Mosurkal, S.; Wang, B.; Zhang, N.; Kaplan, D. L. Silk Degumming Time Controls Horseradish Peroxidase-Catalyzed Hydrogel Properties. *Biomater. Sci.* **2020**, *8* (15), 4176–4185. https://doi.org/10.1039/D0BM00512F.

(34) Sahoo, J. K.; Hasturk, O.; Falcucci, T.; Kaplan, D. L. Silk Chemistry and Biomedical Material Designs. *Nat. Rev. Chem.* **2023**, *7* (5), 302–318. https://doi.org/10.1038/s41570-023-00486-x.

(35) Wittmer, C. R.; Claudepierre, T.; Reber, M.; Wiedemann, P.; Garlick, J. A.; Kaplan, D.; Egles, C. Multifunctionalized Electrospun Silk Fibers Promote Axon Regeneration in Central Nervous System. *Adv. Funct. Mater.* **2011**, *21* (22), 4202. https://doi.org/10.1002/adfm.201190103.

(36) Huang, W.; Rollett, A.; Kaplan, D. L. Silk-Elastin-like Protein Biomaterials for the Controlled Delivery of Therapeutics. *Expert Opin. Drug Deliv.* **2015**, *12* (5), 779–791. https://doi.org/10.1517/17425247.2015.989830.

(37) Shaidani, S.; Jacobus, C.; Sahoo, J. K.; Harrington, K.; Johnson, H.; Foster, O.; Cui, S.; Hasturk,

O.; Falcucci, T.; Chen, Y.; Fletcher, M.; Brooks, C.; Holland, G. P.; Kaplan, D. L. Silk Nanoparticle Synthesis: Tuning Size, Dispersity, and Surface Chemistry for Drug Delivery. *ACS Appl. Nano Mater.* **2023**, *6* (20), 18967–18977. https://doi.org/10.1021/acsanm.3c03451.

(38) Promsuk, J.; Manissorn, J.; Laomeephol, C.; Luckanagul, J. A.; Methachittipan, A.; Tonsomboon, K.; Jenjob, R.; Yang, S.-G.; Thongnuek, P.; Wangkanont, K. Optimizing Protein Delivery Rate from Silk Fibroin Hydrogel Using Silk Fibroin-Mimetic Peptides Conjugation. *Sci. Rep.* **2024**, *14* (1), 4428. https://doi.org/10.1038/s41598-024-53689-7.

(39) Ling, S.; Qin, Z.; Huang, W.; Cao, S.; Kaplan, D. L.; Buehler, M. J. Design and Function of Biomimetic Multilayer Water Purification Membranes. *Sci. Adv.* **2024**, *3* (4), e1601939. https://doi.org/10.1126/sciadv.1601939.

(40) Xin, W.; Zhang, Z.; Huang, X.; Hu, Y.; Zhou, T.; Zhu, C.; Kong, X.-Y.; Jiang, L.; Wen, L. High-Performance Silk-Based Hybrid Membranes Employed for Osmotic Energy Conversion. *Nat. Commun.* **2019**, *10* (1), 3876. https://doi.org/10.1038/s41467-019-11792-8.

(41) Ling, S.; Li, C.; Adamcik, J.; Wang, S.; Shao, Z.; Chen, X.; Mezzenga, R. Directed Growth of Silk Nanofibrils on Graphene and Their Hybrid Nanocomposites. *ACS Macro Lett.* **2014**, *3* (2), 146–152. https://doi.org/10.1021/mz400639y.

(42) Musameh, M. M.; Dunn, C. J.; Uddin, M. H.; Sutherland, T. D.; Rapson, T. D. Silk Provides a New Avenue for Third Generation Biosensors: Sensitive, Selective and Stable Electrochemical Detection of Nitric Oxide. *Biosens. Bioelectron.* **2018**, *103*, 26–31.

(43) Hasturk, O.; Jordan, K. E.; Choi, J.; Kaplan, D. L. Enzymatically Crosslinked Silk and Silk-Gelatin Hydrogels with Tunable Gelation Kinetics, Mechanical Properties and Bioactivity for Cell Culture and Encapsulation. *Biomaterials* **2020**, *232*, 119720. https://doi.org/10.1016/j.biomaterials.2019.119720.

(44) Zheng, H.; Zuo, B. Functional Silk Fibroin Hydrogels: Preparation, Properties and Applications. *J. Mater. Chem. B* **2021**, *9* (5), 1238–1258. https://doi.org/10.1039/D0TB02099K.

(45) Xie, X.; Zheng, Z.; Wang, X.; Lee Kaplan, D. Low-Density Silk Nanofibrous Aerogels: Fabrication and Applications in Air Filtration and Oil/Water Purification. *ACS Nano* **2021**, *15* (1), 1048–1058. https://doi.org/10.1021/acsnano.0c07896.

(46) Hu, Z.; Yan, S.; Li, X.; You, R.; Zhang, Q.; Kaplan, D. L. Natural Silk Nanofibril Aerogels with Distinctive Filtration Capacity and Heat-Retention Performance. *ACS Nano* **2021**, *15* (5), 8171–8183. https://doi.org/10.1021/acsnano.1c00346.

(47) Jin, H. J.; Chen, J.; Karageorgiou, V.; Altman, G. H.; Kaplan, D. L. Human Bone Marrow Stromal Cell Responses on Electrospun Silk Fibroin Mats. *Biomaterials* **2004**, *25* (6), 1039–1047. https://doi.org/10.1016/S0142-9612(03)00609-4.

(48) Ghalei, S.; Mondal, A.; Hopkins, S.; Singha, P.; Devine, R.; Handa, H. Silk Nanoparticles: A Natural Polymeric Platform for Nitric Oxide Delivery in Biomedical Applications. *ACS Appl. Mater. Interfaces* **2020**, *12* (48), 53615–53623. https://doi.org/10.1021/acsami.0c13813.

(49) Pham, D. T.; Tiyaboonchai, W. Fibroin Nanoparticles: A Promising Drug Delivery System. *Drug Deliv.* **2020**, *27* (1), 431–448. https://doi.org/10.1080/10717544.2020.1736208.

(50) Tang-Schomer, M. D.; White, J. D.; Tien, L. W.; Schmitt, L. I.; Valentin, T. M.; Graziano, D. J.; Hopkins, A. M.; Omenetto, F. G.; Haydon, P. G.; Kaplan, D. L. Bioengineered Functional Brain-like Cortical Tissue. *Proc. Natl. Acad. Sci.* **2014**, *111* (38), 13811–13816. https://doi.org/10.1073/pnas.1324214111.

(51) Rnjak-Kovacina, J.; Wray, L. S.; Burke, K. A.; Torregrosa, T.; Golinski, J. M.; Huang, W.; Kaplan, D. L. Lyophilized Silk Sponges: A Versatile Biomaterial Platform for Soft Tissue Engineering. *ACS Biomater. Sci. Eng.* **2015**, *1* (4), 260–270. https://doi.org/10.1021/ab500149p.

(52) Meinel, L.; Hofmann, S.; Karageorgiou, V.; Kirker-Head, C.; McCool, J.; Gronowicz, G.; Zichner, L.; Langer, R.; Vunjak-Novakovic, G.; Kaplan, D. L. The Inflammatory Responses to Silk Films in Vitro and in Vivo. *Biomaterials* **2005**, *26* (2), 147–155. https://doi.org/10.1016/j.biomaterials.2004.02.047.

(53) Wang, Y.; Zheng, Z.; Cheng, Q.; Kaplan, D. L.; Li, G.; Wang, X. Ductility and Porosity of Silk Fibroin Films by Blending with Glycerol/Polyethylene Glycol and Adjusting the Drying Temperature. *ACS Biomater. Sci. Eng.* **2020**, *6* (2), 1176–1185. https://doi.org/10.1021/acsbiomaterials.9b01567.

(54) Wu, J.; Wiggins, R. D.; Weaver, C. H.; Kugel, G.; Kaplan, D. L. Thermoplastic Molding of Silk Protein Composite Plastic Toothbrush Handles with On-Demand Degradability. *Front. Sustain.* **2023**, *4*.

(55) Guo, C.; Li, C.; Vu, H. V; Hanna, P.; Lechtig, A.; Qiu, Y.; Mu, X.; Ling, S.; Nazarian, A.; Lin, S. J.; Kaplan, D. L. Thermoplastic Moulding of Regenerated Silk. *Nat. Mater.* **2020**, *19* (1), 102–108. https://doi.org/10.1038/s41563-019-0560-8.

(56) Falcucci, T.; Radke, M.; Sahoo, J. K.; Hasturk, O.; Kaplan, D. L. Multifunctional Silk Vinyl Sulfone-Based Hydrogel Scaffolds for Dynamic Material-Cell Interactions. *Biomaterials* **2023**, *300*, 122201. https://doi.org/https://doi.org/10.1016/j.biomaterials.2023.122201.

(57) Hu, X.; Kaplan, D.; Cebe, P. Determining Beta-Sheet Crystallinity in Fibrous Proteins by Thermal Analysis and Infrared Spectroscopy. *Macromolecules* **2006**, *39* (18), 6161–6170. https://doi.org/10.1021/ma0610109.

(58) Savvin, S. B. Analytical Use of Arsenazo III: Determination of Thorium, Zirconium, Uranium and Rare Earth Elements. *Talanta* **1961**, *8* (9), 673–685. https://doi.org/https://doi.org/10.1016/0039-9140(61)80164-1.

(59) Park, D. M.; Reed, D. W.; Yung, M. C.; Eslamimanesh, A.; Lencka, M. M.; Anderko, A.; Fujita, Y.; Riman, R. E.; Navrotsky, A.; Jiao, Y. Bioadsorption of Rare Earth Elements through Cell Surface Display of Lanthanide Binding Tags. *Environ. Sci. Technol.* **2016**, *50* (5), 2735–2742. https://doi.org/10.1021/acs.est.5b06129.